BNL-48580

SSN 93-01

MONITORING AND TRACE DETECTION OF HAZARDOUS WASTE AND TOXIC CHEMICALS USING RESONANCE RAMAN SPECTROSCOPY*

A. J. Sedlacek III, D. R. Dougherty and C. L. Chen
Brookhaven National Laboratory
Safeguards, Safety and Nonproliferation Division
Building 197C
Upton, NY 11973

Abstract

Raman scattering is a coherent, inelastic, two-photon process, which shifts the frequency of an outgoing photon according to the vibrational structure of the irradiated species, thereby providing a unique fingerprint of the molecule. When involving an allowed electronic transition (resonance Raman), this scattering cross section can be enhanced by 10^4 to 10^6 and provides the basis for a viable technique that can monitor and detect trace quantities of hazardous wastes and toxic chemicals.

Resonance Raman spectroscopy (RRS) possesses many of the ideal characteristics for monitoring and detecting of hazardous waste and toxic chemicals. Some of these traits are: (1) very high selectivity (chemical specific fingerprints), (2) independence from the excitation wavelength (ability to monitor in the solar blind region), (3) chemical mixture fingerprints are the sum of its individual components (no spectral cross-talk), (4) near independence of the Raman fingerprint to its physical state (very similar spectra for gas, liquid, solid and solutions- either bulk or aerosols), and (5) insensitivity of the Raman signature to environmental conditions (no quenching). Data from a few chemicals will be presented which illustrate these features. In cases where background fluorescence accompanies the Raman signals, an effective frequency modulation technique has been developed, which can completely eliminate this interference.

Introduction

With our increased environmental awareness has come the need for technologies that can detect, identify and monitor pollutants and, where necessary, verify their destruction. This need is evidenced by the recent (late 1990) creation of the Clean Air Act Amendments (CAAA), of which the Title III-Hazardous Air Pollutants (HAP) amendments mandate the complete revision and expansion of the earlier Clean Air Act (CAA), section 112.[1] As was pointed out by Grant, Kagann and McClenny,[2] optical remote sensing technologies are expected to play a very important role in insuring that various facilities are in compliance with the Maximum Achievable Control Technology (MACT) standards for the reduction of HAP emissions that are called for in section 301 of Title III. Unfortunately, many of these technologies have varying detection and applicability characteristics which often dictate the conditions under which one can use the sensor to monitor, detect, identify or verify a chemical species. Although the report by Grant et al.[2] is informative and illustrative of the potential of remote detection and identification of toxic gases, it is, however, limited to open-path optical *absorption* techniques. The remote sensing instruments examined in their report included Fourier Transform Infrared spectroscopy (FTIR), differential optical absorption spectroscopy (DOAS), laser long-path absorption, differential absorption LIDAR (DIAL) and gas-cell correlation spectroscopy. In this paper we will introduce the optical technique of resonance Raman LIDAR for the remote detection, monitoring, identification and verification of toxic chemicals. This inelastic scattering technology, although not absorption, is a natural extension to Grant, Kagann and McClenny's[2] paper in that this is an *open-path*, remote-sensing technique. Resonance Raman LIDAR is an improvement on the above cited technologies, save FTIR, in that optical fingerprints are at the heart of Raman spectroscopy. Fingerprinting has the obvious advantage that no prior knowledge is required of which chemicals are to be interrogated, as is *required* for both DOAS and DIAL (i.e., need to know the absorption maximum location so that one laser can be tuned to this maximum and the second detuned)[3] and because the optical signature *is* species specific. Furthermore, Raman scattering has the advantage that the spectral fingerprint is not obscured by water as is the case for both dispersive- and FT-infrared spectroscopy. Some of the other advantages[4-9] that a Raman sensor possess are: (1) very high selectivity (chemical specific fingerprints), (2) independence from the excitation wavelength (ability to monitor in the solar blind region), (3) chemical mixture fingerprints are the sum of its individual components (no spectral cross-talk), (4) near independence of the Raman fingerprint to its physical state (very similar spectra for gas, liquid, solid and solutions), and (5) insensitivity of the Raman signature to

*This work was performed under the auspices of the U.S. Department of Energy, Contract No. DE-AC-02-76CH00016

environmental conditions (no quenching, or interference from water). Resonance Raman spectroscopy can offer the fingerprinting advantage coupled with high sensitivity for trace analysis, providing a very powerful technique for detecting, identifying, monitoring, and, in the case of destruction, verifying many classes of chemicals.

Unfortunately, the inherently small scattering cross-sections for normal Raman have effectively precluded the use of the technology outside of the lab. However, when the excitation frequency approaches an electronically excited state of the molecule[6,9,12-16], an enormous enhancement of the scattering cross-section can occur, often up to 4 to 6 orders of magnitude, and is referred to as resonance Raman (RR), since the excitation frequency is in "resonance" with an allowed electronic transition. This improvement in the cross-section, in conjunction with the global advantages of Raman spectroscopy cited earlier, provide a promising optical open-path platform for the remote sensing of toxic chemicals and hazardous wastes. In addition, because water is a poor Raman scatterer, the measured Raman fingerprint is invariant to environmental perturbations. Furthermore, this scattering technique has equal applicability to gases, liquids, solids, and solutions.

Theory of Normal and Resonance Enhanced Raman Intensities

The fundamental equation which describes the Raman intensity[5,710,12] under *normal* scattering conditions is

$$I = K(\nu_o - \nu_{kl}) I_o \sum_{\rho\sigma} \left| \left(\alpha_{\rho\sigma}\right)_{GF} \right|^2 \tag{1}$$

where K is a constant, I_o is the incident light intensity (photons $sec^{-1}cm^{-2}$), ν_o is the frequency of the incident light wave, ν_{kl} is the vibrational frequency, and $\left(\alpha_{\rho\sigma}\right)_{GF}$ is the transition polarizability tensor which, derived from second-order perturbation theory, is

$$\left(\alpha_{\rho\sigma}\right)_{GF} = \frac{1}{\hbar} \sum_{I} \left(\frac{\langle F|\mu_\rho|I\rangle\langle I|\mu_\sigma|G\rangle}{\nu_{GI} - \nu_o + i\Gamma_I} + \frac{\langle I|\mu_\rho|G\rangle\langle F|\mu_\sigma|I\rangle}{\nu_{IF} + \nu_o + i\Gamma_I} \right) \tag{2}$$

where the transition involves $|G\rangle, |F\rangle$, and $|I\rangle$, the initial, final and intermediate states, respectively, ρ and σ are the incident and scattered polarizations, Γ_I is a dampening factor reflecting the homogeneous width of state $|I\rangle$ and μ is the electron position operator. A very important result of Eqn. 2 is that as the laser energy, ν_o, approaches the energy of an allowed molecular transition, ν_{GI}, the denominator, $\nu_{GI} - \nu_o + i\Gamma_I$, becomes very small and the first term in the sum dominates, thereby making $\left(\alpha_{\rho\sigma}\right)_{GF}$ very large: this is the *resonance* condition. It is important to understand that other factors, such as symmetry, add further requirements which mediate the strength of the resonance enhancement, but in principle, every molecule will have the resonance condition satisfied when excited with radiation whose energy is close to an electronic transition of the species. Since I has the units of photons/sec, the ratio I/I_o gives the Raman scattering cross-section (units are cm^2).

Albrecht and Hutley[17] derived an expression for the polarizability having two major components such that the frequency dependence of the Raman intensity can be understood. The first term, corresponding to their A-term in the polarizability, has the following frequency dependence in scattering intensity

$$I \propto \left(\nu_o \pm \nu_{kl}\right) \left[\frac{\nu_e^2 + \nu_o^2}{\left(\nu_e^2 - \nu_o^2\right)^2} \right]^2 = F_A, \tag{3}$$

which is often referred to as the Franck-Condon factor term, where ν_e is the frequency of the resonant excited state . The A-term presupposes the existence of *one* electronic state being responsible for the resonance enhancement.

The second term of the polarizability tensor corresponds to Albrecht and Hutley's B-term which deals with a weakly allowed transition gaining intensity from a nearby strongly allowed transition. The frequency dependence of this term is described as

$$I \propto 4(\nu_o \pm \nu_{kl})\left[\frac{\nu_e \nu_s + \nu_o^2}{(\nu_e^2 - \nu_o^2)(\nu_s^2 - \nu_o^2)}\right]^2 = F_B, \quad (4)$$

where ν_S is the frequency of the second electronic transition. In addition to being called the B-term, this term is also commonly referred as the Herzberg-Teller term.[5]

Under what conditions[2,5,6] does one term dominate? Generally speaking, the necessary conditions are reasonably well defined. When the transition matrix element is large and the excited-state potential function is shifted significantly from the ground-state equilibrium position and has a different shape, then the expected dominant factor is the Franck-Condon overlap (i.e., A-term); that is to say, there must be a large force-constant change associated with the excited state. Under these conditions, the relative intensities are governed by the overlap of vibrational states and consequently overtones can have significant intensity. Also, in order for the matrix element to be non-zero, it must be invariant to all symmetry operations of the molecular symmetry group, consequently, only totally symmetric vibrations will be enhanced. When the laser frequency is in resonance with a weakly allowed transition, significant enhancement can be observed if there is a nearby strongly allowed transition from which intensity may be borrowed. Under these circumstances, the second term will dominate because the Herzberg-Teller interaction will be larger than the Franck-Condon interaction. The major consequence of this term is that both non-totally symmetric and totally symmetric modes will undergo enhancement. This broad enhancement results because the intermediate state no longer needs to be totally symmetric. Finally, in the limit that an excited state's potential energy surface is similar to the ground state (which is often the case), the Franck-Condon overlap will result only in Rayleigh scattering. Under these conditions, the B-term is expected to dominate over the A-term since the vibrational overlap will be very small.

Experimental Arrangement

Since our RR experimental setup follows in spirit the general arrangement throughout the spectroscopy community[13-16], only a very brief overview will be given here. Essentially the output from a dye laser pumped by an excimer laser is sent into a 1-mm quartz liquid cell. Both Rayleigh and Raman scattering is collected in the 90° configuration (we can, with equal efficiency, change the arrangement to a 180° backscattering configuration) by a doubling grating SPEX monochromator (2400 grooves/mm) and detected by an optical multichannel analyzer (OMA: EG&G). The digitized signal from the OMA is then sent to a Macintosh IIfx computer for storage and later analysis using National Instruments LabVIEW® software. We are currently conducting experiments on liquids but can readily replace this liquid cell with a gas cell.

Results and Discussion

In order to assess the potential of a resonance Raman LIDAR sensor, it is necessary to first measure the scattering cross-sections of the set of chemicals of interest as a function of excitation wavelength. This measurement can be done either absolutely or relative to a standard. The former is nontrivial and requires great care in alignment of the optics, measurement of the photon fluence/flux, corrections for reflective or absorption losses and quantum efficiencies of the detector and monochromator. A much simpler approach is to employ a known standard, whose inelastic scattering cross-section is known as a function of excitation wavelength, and then measure the Raman scattering cross-section of the unknown against the known. We have taken the latter approach in our laboratory because absolute cross-sections, at specific wavelengths, are available for the solvents that are to be employed. We have chosen three solvents of varying polarities to insure that all chemicals of interest can be interrogated properly; cyclohexane (C_6H_{12}); dichloromethane (CH_2Cl_2); and acetonitrile (CH_3CN). For the present paper, the discussion will be limited to cyclohexane and acetonitrile.

Figures 1a and 1b show the fingerprint region of cyclohexane following irradiation at 440 nm and 220 nm, respectively. Also shown, in the inset 1a, is the ultraviolet absorption of cyclohexane. The striking feature between these two spectra is that the 802 cm^{-1} peak appears to grow weaker as the excitation is shifted to shorter wavelengths. Instead, however, the other modes of cyclohexane are undergoing a significant *pre-resonance* enhancement. Following this initial finding, we then measured the differential Raman scattering cross-sections for the 802 cm^{-1} and 1028 cm^{-1} peaks as a function of excitation wavelength

$$\frac{d\sigma_R(\lambda)}{d\Omega} = \varepsilon(\bar{\nu} - \bar{\nu}_o)^4 \frac{d\sigma_R(\lambda_o)}{d\Omega}, \quad (5)$$

where $d\sigma_R(\lambda)/d\Omega$ is the differential cross-section at an excitation wavelength of λ, $\bar{\nu}_o$ is the wavenumber equivalent for 436 nm, $\bar{\nu}$ is the excitation wavelength in wavenumbers, and ε is the resonance enhancement.

This equation accounts for the well-known ν^4 dependence of the Raman cross-section on excitation frequency. The results of these experiments are collected in Figure 2. Also shown in this figure are the results of previous investigations[18-22] along with the predicted fourth-power dependence of the cross-section (both the data and the predicted fourth-power dependence are normalized to 1 at 436 nm). At about 270 nm it can be clearly seen that both modes are undergoing an enhancement beyond the expected ν^4-dependence. In addition, it can also be seen that the 1028 cm^{-1} peak of cyclohexane undergoes a total enhancement of 613 times as opposed to only 60 times for the 802 cm^{-1} peak; this accounts for the change in the relative intensities seen in Figure 1. The 1028 cm^{-1} peak, also normalized to 1 at 436 nm, is ultimately referenced to the 802 cm^{-1} peak since no work has been done on this particular mode of cyclohexane.

In an effort to understand more completely the mechanism responsible for the observed enhancement, the cyclohexane data were fit to Albrecht's A-term and B-term[17] (Eqns. 3 and 4). However, fitting these 802 cm^{-1} data to Albrecht's B-term was unsuccessful. The 802 cm^{-1} data set was then fit to a modified version of the A-term in order to account for a frequency-independent contribution to the enhancement in accord with that suggested by Asher.[11] Plotted on the same graph in Figure 3a is the predicted ν^4-dependence of the Raman intensity. As is readily observable, the fit to the modified Albrecht A-term is quite good and shows how the enhancement becomes greater as the excitation energy approaches resonance with the allowed electronic transition. Since the modified A-term slightly underestimates the energy of the lowest electronic state and the original A-term slightly overestimates its value, the energy of the lowest electronic state that couples to this mode is taken as the average from these two extremes. The energy of the lowest electronically excited state that couples to the 802 cm^{-1} vibration is estimated to be ~82500 cm^{-1}. An examination of the vacuum ultraviolet (VUV) spectrum[23] of cyclohexane reveals that a strongly allowed σ-σ^* (CC) transition occurs between 75000 cm^{-1} and 95000 cm^{-1} and is probably responsible for the pre-resonance enhancement that is observed.

Since the data set for the 1028 cm^{-1} vibration was not nearly as complete as for the 802 cm^{-1} vibration, this mode was fit to only the A-term. As is clearly observed in Figure 3b, the curve fitting is at best marginal. This probably results from (1) too few data over the large range of excitation energies used in the fit and (2) because the energy of the lowest electronic state that couples to this mode is predicted to be ~57700 cm^{-1} and therefore this mode is probably undergoing a resonance enhancement and the approximations used to derive the A-term are no longer valid. The A- and B-terms were derived in the pre-resonance limit and therefore will probably break down when the resonance condition is satisfied. A transition centered around 63000 cm^{-1} is the most likely candidate responsible for this mode's enhancement. Fits to the other functional forms did not result in any significant improvement in the fit.

The resonance enhancement of acetonitrile[24] in the UV is even more impressive. Collected in Figure 4 is the C-H stretching region of CH_3CN as a function of 3 excitation wavelengths, 440, 225 and 220 nm. On the scale displayed for the 440 nm results, the ν_5 mode of CH_3CN is not even visible; however, at 225 nm it is of nearly equal intensity to the ν_1 mode, and a reduction of the excitation wavelength of only 5 nm results in a further dramatic enhancement of this mode. Calibration of the area under this transition to the 973 cm^{-1} mode reveals that the ν_5 mode undergoes an enhancement in excess of 10^6, resulting in a total resonance enhanced scattering cross section of ~1×10^{-23} cm^2. Although we have not yet mapped out this mode's resonance enhancement, several strong broad absorption features exist just below ~170 nm and represent the most likely transitions responsible for the huge enhancement. Current research effort is aimed at mapping out the frequency dependence of the scattering cross-section in order to obtain an estimate of the energy of the lowest electronic state that couples to this mode. In addition, twelve other organic and inorganic compounds have been examined and all exhibit 10^3 to 10^6 orders of magnitude enhancement for the differential scattering cross-section.

Resonance Raman LIDAR

The whole purpose of measuring the resonance Raman cross-sections is to estimate the potential for a resonance Raman LIDAR remote sensor. Since this phenomenon is inherently a scattering process, its extension to the remote detection of effluents should be straightforward with the only critical requirement being the size of the resonance Raman scattering cross-section. To properly evaluate the potential of this extension, we have examined the LIDAR signal dependence under a variety of conditions using the following LIDAR signal equation,[2,25]

$$S = 2.69\times10^5\,\eta N \frac{E}{\hbar\nu_o}\frac{AL}{R^2}\rho\frac{d\sigma}{d\Omega}\left[\exp-(\alpha_s+\alpha_o)R\right], \qquad (6)$$

where η is the total detection efficiency, N the number of pulses, E the laser pulse energy, ν_0 the laser frequency, A the collector area (cm^2), L the range increment (m), R the range (km), and α_0 and α_s the atmospheric absorption coefficients at the laser and scattering frequencies. The numerical factor out in front of the equation allows the concentration of the species, ρ, to be expressed in ppm and $d\sigma/d\Omega$ is the RR differential scattering cross-section. For the following assessment, we have assumed a 5% total collection efficiency at a laser wavelength of 266 nm (quadrupled Nd:YAG laser) at a repetition rate of 500 Hz, with a collector area of $\sim 10^4$ cm^2 and a visibility of 23 km. We evaluated Eqn. 6 under a signal-to-noise (S/N) ratio of 10 ($\sqrt{S}$). Other factors used are collected in Table I.[26]

Shown in Figure 5a is the sensitivity of a UVRR LIDAR remote sensor as a function of both range and integration time. It can be seen that integrating scattered light for 60 seconds from a stack 1 km away with a differential cross-section of 7×10^{-25} cm^2/sr will allow detection of an effluent at the sub-ppm·m level. Alternatively, at a distance of 5 km, the effluent could be detected at the low ppm·m level. Even with an integration time as short as 10 seconds, ppm·m could easily be detected at a distance of 1 km. Displayed in Figure 5b is the RR LIDAR sensitivity as a function of both range and differential scattering cross-section. Here we can see that even when the differential cross-section is as small as 10^{-27} cm^2/sr and the laser pulse energy is as low as 10 mJ, the detection concentration, with 60 seconds integration time, is at the 100s ppm·m level. The ability to use laser excitation below 300 nm is significant because interrogation of a plume can be done during the day without necessary solar background corrections that would otherwise be required. Of course, care must be taken when working in the UV because of the strongly absorbing ozone.

Melfi[27-28] of NASA and others[29-33] have employed a normal Raman LIDAR system to probe/monitor water vapor in the atmosphere from ground level up to 13 km from a ground-based system. In Melfi's LIDAR system, a XeF excimer laser operating at 351 nm is employed and a series of bandpass filters are used to isolate spectral regions for water (3000-4000 cm^{-1}), O_2 and N_2. His success suggests that a resonance Raman-based LIDAR system should offer great potential, especially in light of the fact that the differential scattering cross-section for water is only $\sim 10^{-29}$ cm^2/sr and the differential scattering cross-sections typically found for molecules with pre-resonance or resonance enhancement range from 10^{-26} cm^2/sr to 10^{-23} cm^2/sr. Further evidence is provided by the series of studies conducted by Hirschfeld et al.[34] in the early 1970s where the potential of normal Raman LIDAR was demonstrated by monitoring SO_2, CO_2, H_2O and kerosene emissions from a stack. In this project, a doubled ruby laser (λ_{exc}=347.15 nm) was employed along with the state-of-the-art photomultiplier tubes (PMT) and collection optics. Using a range resolution of 10 m, their instrument could measure the concentration of SO_2 at 30 ppm·m and kerosene at 1.7 ppm·m at a distance of 200 m with a 36 inch collection optic. These results were without the aid of resonance enhancement, which would lower the detection limits or increase the monitoring range.

Conclusions and Prognosis

We have discussed the potential of resonance Raman LIDAR as a remote sensor that can be used for gases, liquids or solids. This spectroscopy has the fundamental advantage that it is based on optical fingerprints that are insensitive to environmental perturbations or excitation frequency. By taking advantage of resonance enhancement, the inelastic scattering cross-section can increase anywhere from 4 to 6 orders of magnitude which translates into increased sensing range or lower detection limits. It was also shown that differential cross-sections as small as 10^{-27} cm^2/sr do not preclude the use of this technique as being an important component in one's remote-sensing arsenal. The results obtained in the early 1970s on various pollutants and the more recent work on atmospheric water cast a favorable light on the prospects for the successful development of a resonance Raman LIDAR. Also, since a large fraction of the chemicals related to waste management and environmental restoration have near UV and visible absorptions, it is expected that many will have pronounced resonance enhancements.

Acknowledgements

The authors wish to thank James Marecek (State University of New York at Stony Brook) for synthesis and purification of these and other chemicals and David Harder for his technical support. This research was sponsored by the Systems and Technology Division of the Office of Arms Control and Nonproliferation, U.S. Department of Energy.

References:

1 Lee, B., J. Air Waste Manage. Assoc. **41**, 16 (1991).

2. Grant, W. B., Kagann, R. H. and McClenny, W. A., J. Air Waste Manage. Assoc. **42**, 18 (1992).

3 Measures, R. M., Laser Remote Chemical Analysis, in *Chemical Analysis Series Vol. 94*, R. M. Measures, Ed., John Wiley and Sons: New York 1988.

4. Hendra, P., Jones, C. and Warnes, G., *Fourier Transform Raman Spectroscopy: Instrumentation and Chemical Applications*, Ellis Horwood: New York 1991.

5 Grasselli J. G. and Bulkin B. J., *Analytical Raman Spectroscopy*, John Wiley and Sons: New York 1991.

6. Carey, P. R., *Biochemical Applications of Raman and Resonance Raman Spectroscopies*, Academic Press: New York 1982.

7. Schrötter, H. W. and Klöckner H. W., Raman Spectroscopy of Gases and Liquids in *Topics in Current Physics*, A. Weber, Ed., Springer-Verlag: New York 1979.

8. Long D. A., *Raman Spectroscopy*, McGraw-Hill: New York 1977.

9. Nelson, W. H. and Sperry, J. F., *Modern Techniques for Rapid Microbiological Analysis*, W. H. Nelson, Ed., VCH Publishers: New York 1991.

10. Wilson Jr., E. B., Decius, J. C. and Cross, P. C., *Molecular Vibrations*, Dover Publications: New York 1955.

11. Siegman, A. E., *Lasers*, University Science Books: Mill Valley, CA 1986.

12. Rousseau, D. L., Friedman, J. M. and Williams, P. F., Raman Spectroscopy of Gases and Liquids in *Topics in Current Physics*, A. Weber, Ed., Springer-Verlag: New York 1979.

13. Asher, S. A., Anal. Chem. **56**, 720 (1984).

14. Asher, S. A., *Ann. Rev. Phys. Chem.* **39**, 537 (1988).

15. Ziegler, L. D. and Albrecht, A. C., J. Chem. Phys. **70**, 2634 (1979).

16. Hirakawa, A. Y. and Tsuboi, M., Science **188**, 359 (1975).

17. Albrecht, A. C. and Hutley, M. C., J. Chem. Phys. **55**, 4438 (1971).

18. Trulson, M. O. and Mathies, R. A., J. Chem. Phys. **84**, 2068 (1986).

19. Colles, M. J. and Griffiths, J. E., J. Chem. Phys. **56**, 3384 (1972).

20. Murphy, W. F., Holzer, W. and Bernstein, H. J., Appl. Spectrosc. **23**, 211 (1969).

21. Abe, N., Wakayama, M., and Ito, M., J. Raman Spectrosc. **6**, 38 (1977).

22. Nestor, J. R. and Lippincott, E. R., J. Raman Spectrosc. **1**, 305 (1973).

23. Raymonda, J. W. and Simpson, W. T., J. Chem. Phys. **47**, 430 (1967).

24. Dudik, J. M., Johnson, C. R. and Asher, S. A., J. Chem. Phys. **82**, 1732 (1985).

25. Rosen, H., Robrish, P. and Chamberlain, O., Appl. Optics **14**, 2703 (1975).

26. Scattering data taken from "Optical Properties of the Atmosphere", AFCRL-72-0497, 24 August 1972.

27. Melfi, S. H., Appl. Optics **11**, 1605 (1972).

28. Melfi, S. H., Koutsandreas, J. D. and Moran, J., Environ. Sci. Technol. **11**, 36 (1977).

29. Bilbe, R. M., Bullman, S. J. and Swaffield, F., Meas. Sci. Technol. **1**, 495 (1990).

30. Riebesell, M., Voss, E., Lahmann, W., Weitkamp, C. and Michaelis, W., *Proc. Int. Conf. Lasers*, **1987**, 129.

31. Cooney, J., Petri, K. and Salik, A., Appl. Opt. **24**, 104 (1985).

32. Petri, K., Salik, A. and Cooney, J., Appl. Opt. **21**, 1212 (1982).

33. Renaut, D., Pourny, J. C. and Capitini, R., Opt. Lett. **5**, 233 (1980).

34. Hirschfeld, T., Schildraut, E. R., Tannenbaum, H. and Tanenbaum, D., Appl. Phys. Lett. **22**, 38 (1973).

TABLE I: Parameters Employed for Resonance Raman LIDAR Evaluation

Parameter	Value (or Range)
Detection efficiency (η)	5%
Number of laser pulses (N)	repetition rate: 500 Hz
Laser pulse energy (E)	0.1-100 mJ
Laser frequency/wavelength (ν_o)	260 nm
Collector area (A)	~10^4 cm^2
Range increment (L)	4.5 m
Atmospheric abs. coeff. @ laser frequency (α_o)	0.3 km^{-1}
Atmospheric abs. coeff. @ scattered frequency (α_s)	0.3 km^{-1}

Figure captions:

Figure 1:

Spectral fingerprint of cyclohexane following irradiation at 440 nm and 220 nm. Inset is the UV absorption spectrum of liquid cyclohexane. Whereas the transition located at the Raman shifted frequency 802 cm^{-1} undergoes an enhancement of 60 times, the transition at 1028 cm^{-1} is enhanced more than 600 times.

Figure 2:

A plot of the areas under the peaks located at the Raman-shifted frequencies 802 cm^{-1} and 1028 cm^{-1} as a function of excitation wavelength. Solid symbols are results obtained in this laboratory and open squares are the results from other studies. Also shown is the ν^4-dependence of the Raman intensity on excitation frequency. All data are normalized to 1 at 436 nm.

Figure 3:

a)

The results of curve fitting the experimental data for the Raman-shifted transition at 802 cm^{-1} to a modified version of Albrecht's A-term. Solid circles are from the present investigation and open circles are from previous investigations. Also shown is the ν^4-dependence of the Raman intensity on excitation energy. The onset of pre-resonance enhancement is observable around 270 nm (~37000 cm^{-1}).

b)

The results of curve fitting the experimental data for the Raman-shifted transition at 1028 cm^{-1} to Albrecht's A-term. Also shown is the ν^4-dependence of the Raman intensity on excitation energy. The enhancement is approaching 3-4 orders of magnitude as the excitation energy comes into resonance with the electronic state that couples to this mode.

Figure 4:

The ν_1 and ν_5 C-H stretching modes of acetonitrile as a function of laser excitation wavelength. At 440 nm excitation, the ν_5 mode is not even visible, whereas at 225 nm it is of nearly equal intensity as the ν_1 mode. Changing the excitation wavelength by just 5 nm results in a dramatic increase in the ν_5 mode's scattering cross-section.

Figure 5:

a)

Resonance Raman LIDAR sensitivity as a function of temporal integration and range. As can be seen, sub ppm·m concentrations can be detected with 60 seconds integration. Alternatively, 10 seconds integration is enough time to detect ppm·m at 1 km from the origin.

b)

Resonance Raman LIDAR sensitivity as a function of differential cross-section and range. It can be seen that a differential cross-section as small as 10^{-27} cm^2/sr does not preclude the value of resonance Raman LIDAR for remote detection of effluents.

Cyclohexane Fingerprint

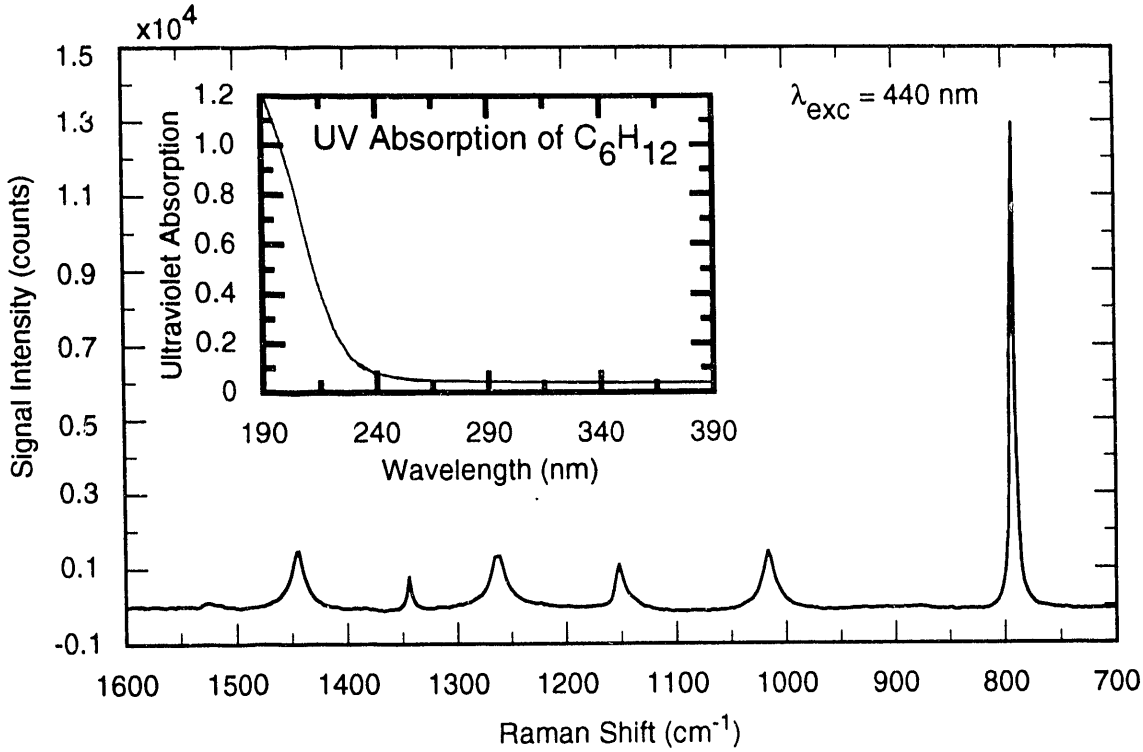

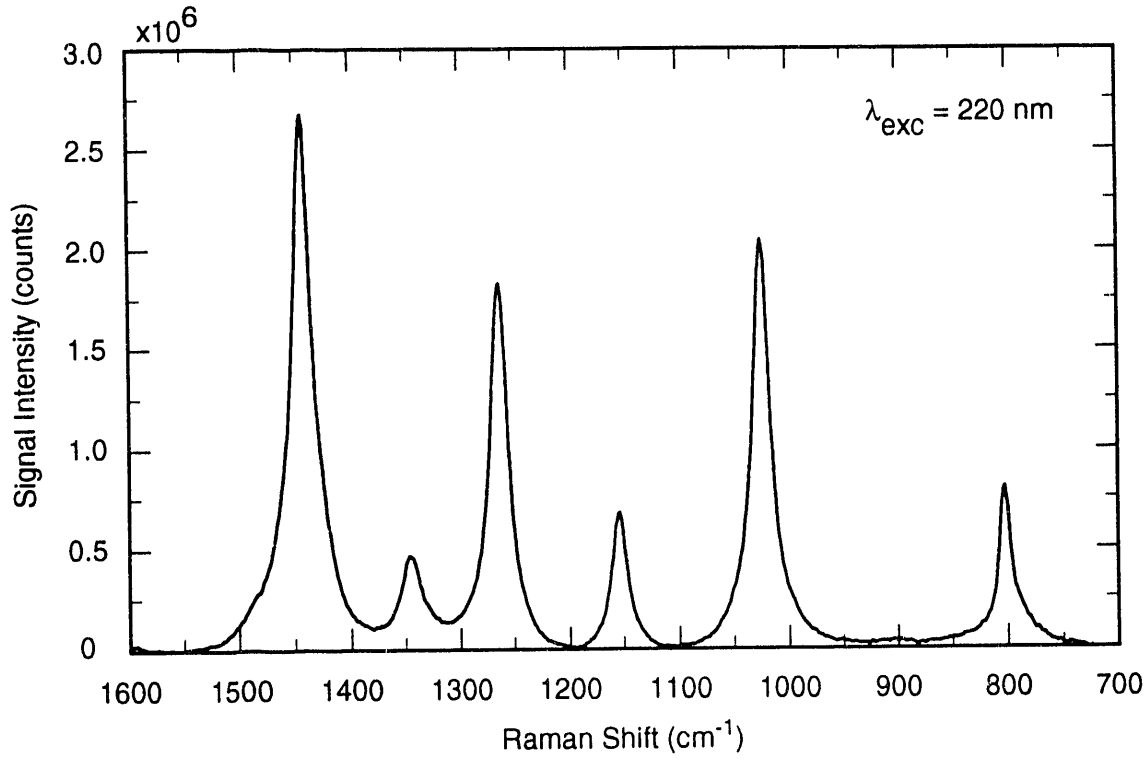

802 cm^{-1} and 1028 cm^{-1} Raman Cross-Sections vs. Laser Excitation Wavelength

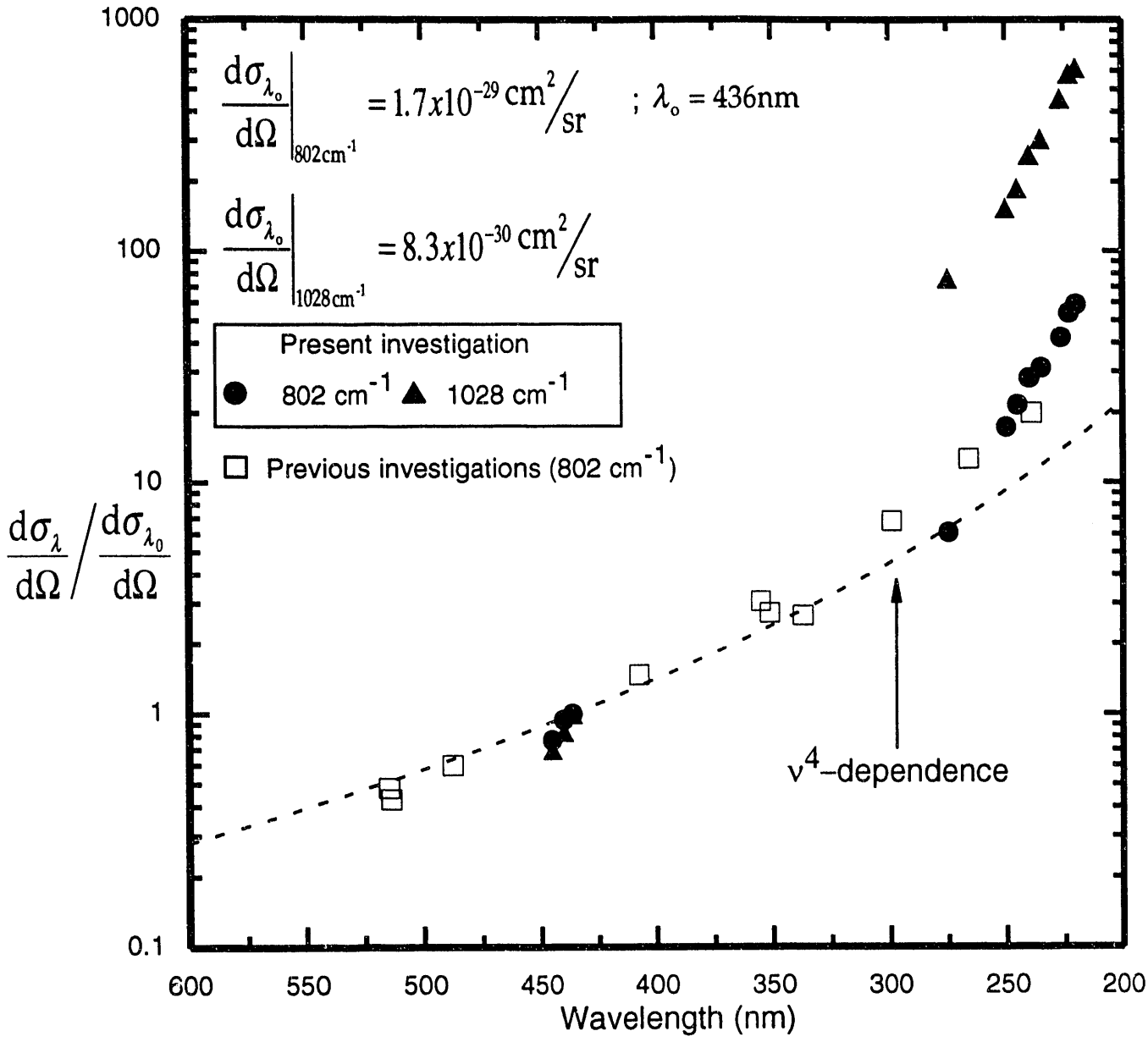

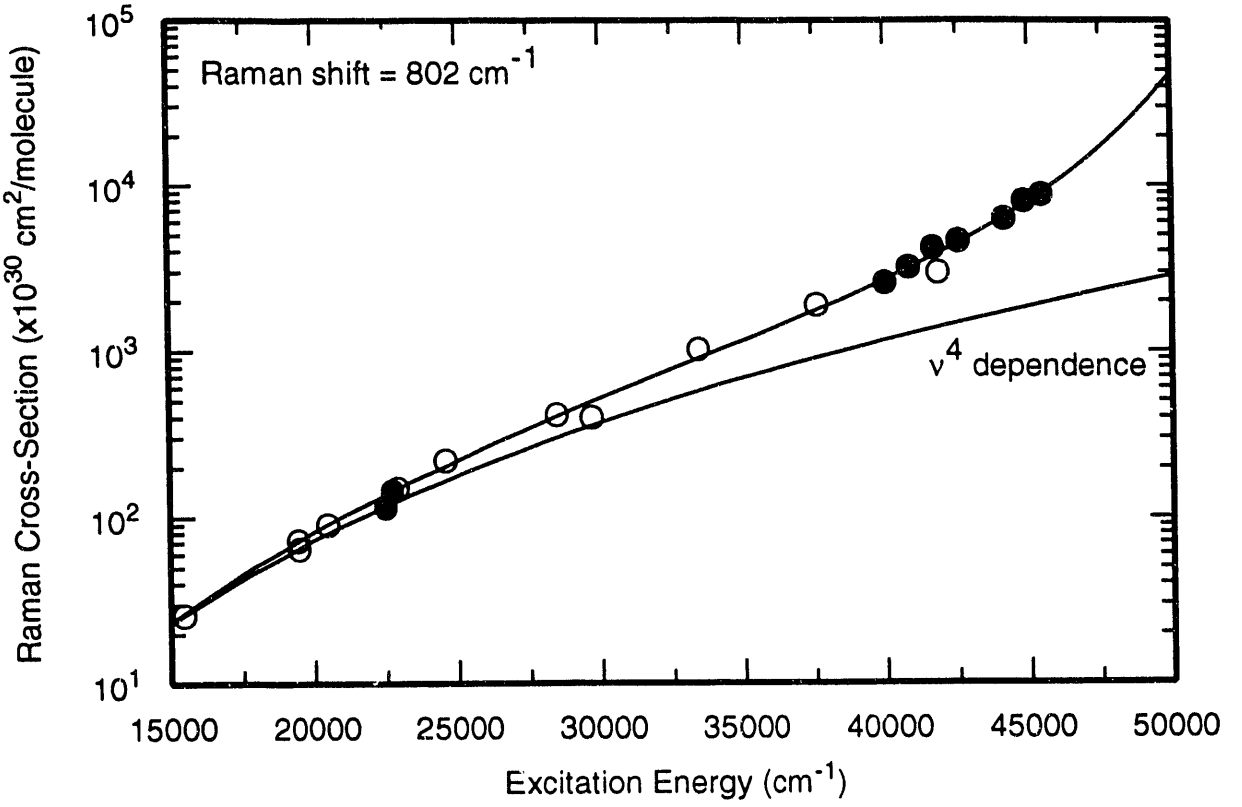
Raman shift = 802 cm^{-1}
ν^4 dependence
Raman Cross-Section (x10^{30} cm^2/molecule)
Excitation Energy (cm^{-1})
10^5
10^4
10^3
10^2
10^1
15000
20000
25000
30000
35000
40000
45000
50000

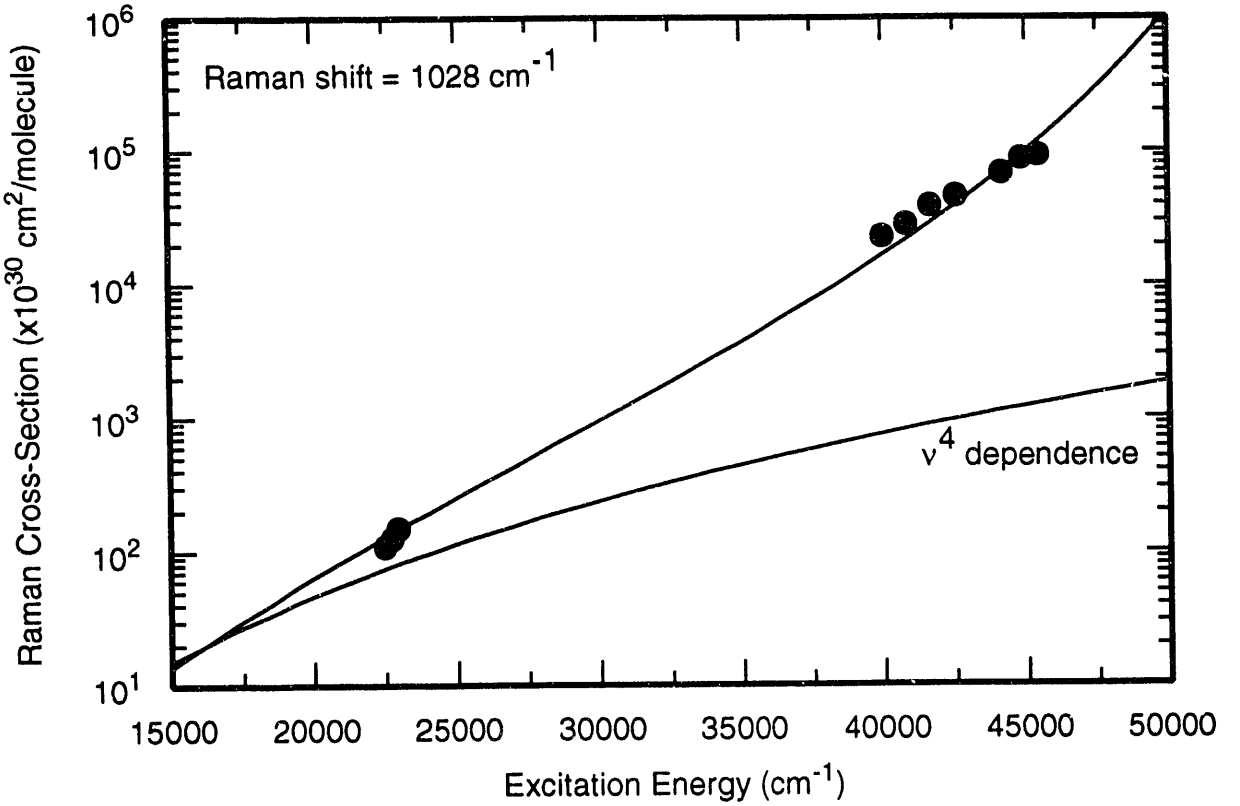
Raman shift = 1028 cm^{-1}
ν^4 dependence
Raman Cross-Section (x10^{30} cm^2/molecule)
Excitation Energy (cm^{-1})
10^6
10^5
10^4
10^3
10^2
10^1
15000
20000
25000
30000
35000
40000
45000
50000

ν_1 and ν_5 C-H Stretching Modes of CH_3CN as a Function of Laser Excitation Wavelength

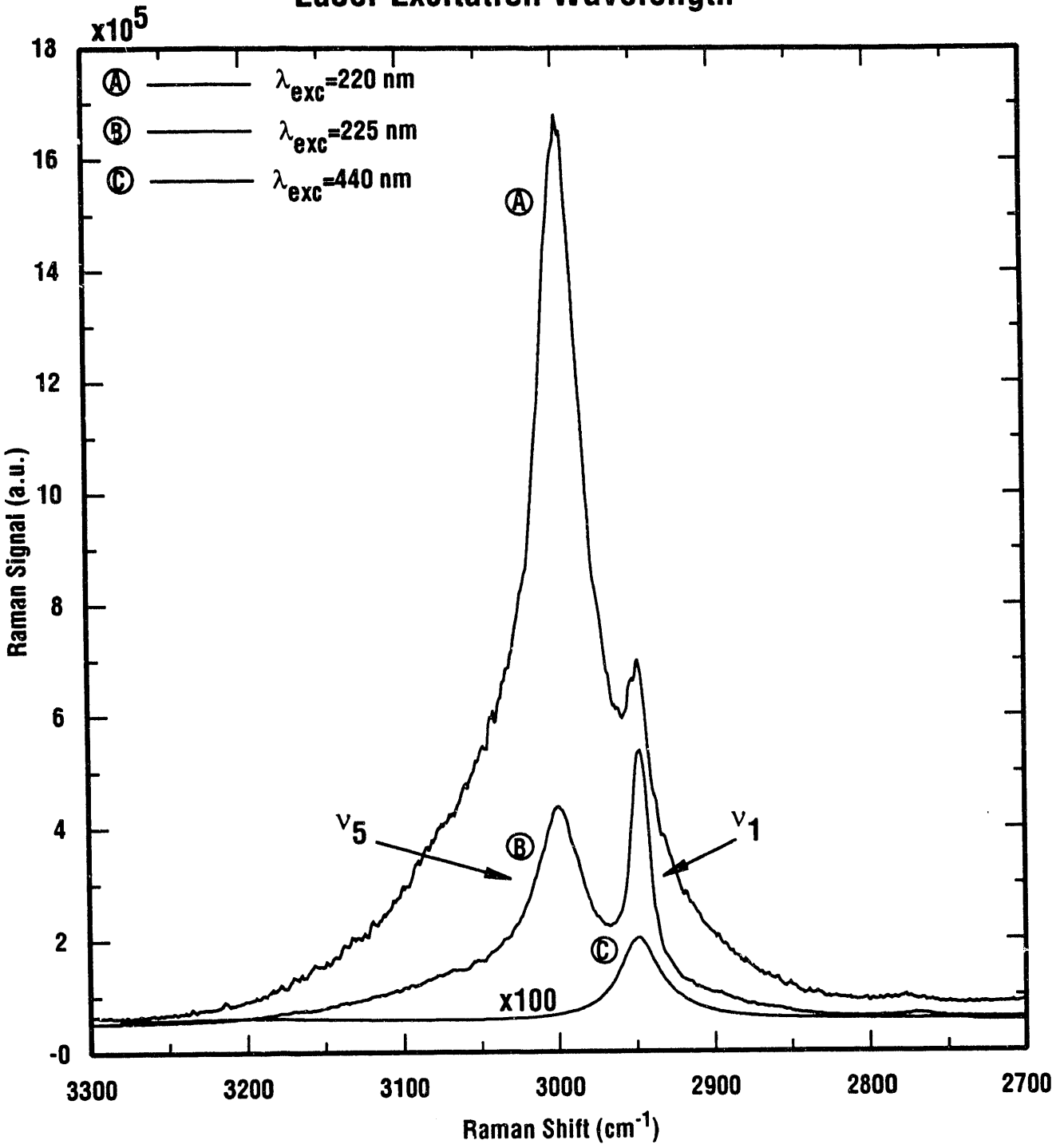

- Resonance Raman may have 10^4 to 10^6 enhancement factor over that of the normal Raman cross-section

LIDAR Sensitivity vs. Range: Temporal Integration Dependence

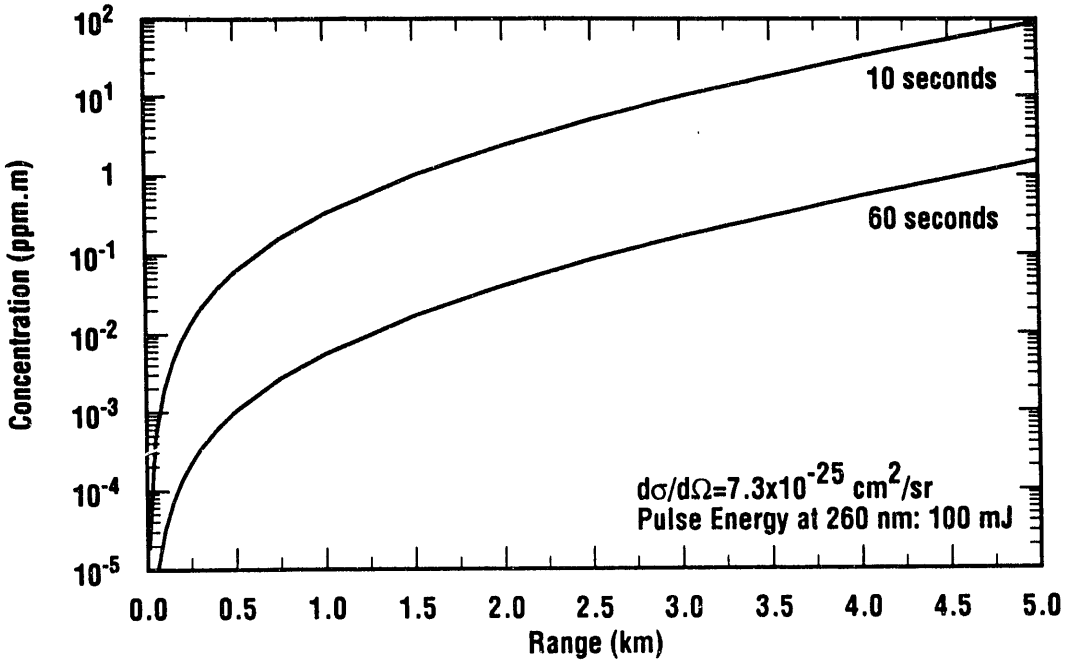

LIDAR Sensitivity vs. Range: Differential Cross-section Dependence

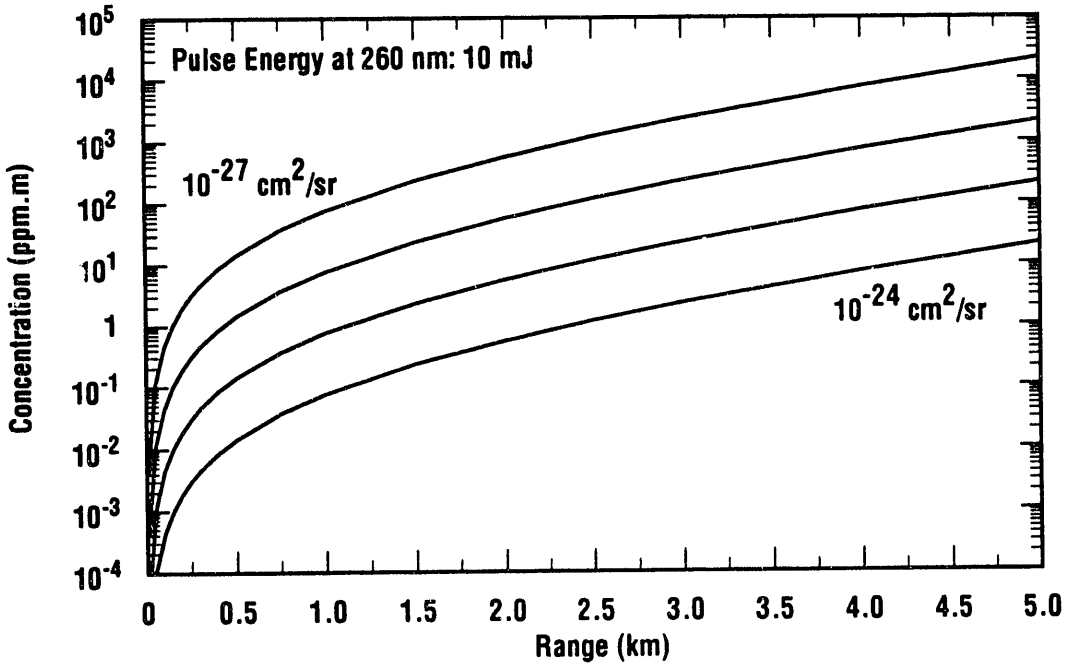

END

DATE
FILMED
7/21/93